Computational Simulation of Fluid and Dilute Particulate Flows on Spiral Concentrators

B.W. Matthews[1], C.A.J. Fletcher[1] and A.C. Partridge[2]

1. Centre for Advanced Numerical Computation in Engineering and Science
2. Centre for Minerals Engineering
University of New South Wales, Sydney 2052, Australia

ABSTRACT

Spiral concentrators are used in the fine coal and mineral processing industries to segregate, by gravitation, particles on the basis of density and size. To optimise the spiral geometric parameters towards enhanced performance, the past decade has seen developments in theoretical predictions of spiral flow characteristics. To this end, this paper uses Computational Fluid Dynamics (CFD) analysis to simulate fluid and dilute particulate flows on one spiral unit used for fine coal processing. The free-surface Volume-of-Fluid (VOF) algorithm, RNG k-ε turbulence model and Lagrangian method have been used for this purpose. Results have been compared with primarily an associated experimental program, and the present model forms the basis for future examination of the two-way fluid-particle coupling processes and inter-particle effects.

1. INTRODUCTION

The generic geometry of spiral concentrators consists of an open trough that spirals vertically downwards in helix configuration about a central axis. Employed in the fine coal and mineral processing industries, a slurry of fine particles (75 - 3000 μm) is fed to the top of the spiral and, as it gravitates downwards, particles are segregated radially across the trough by the centrifugal force. Since their introduction to Australia in the 1940's, evolution of the design has been almost exclusively based on empirical development of the appropriate geometry. However, this approach has proven to be expensive and time-consuming. The past decade has therefore seen developments in theoretical flow investigations, of which CFD has particular potential benefit because the detailed flow and particle interactions in complex geometries can be solved using only the fundamental governing flow equations.

Following Wang and Andrews (1994), who used CFD to determine the flow fields for simplified rectangular spiral sections, Jancar *et al.* (1995) examined the fluid flow on the coal-concentrating LD9 spiral using their locally developed code. As part of an ongoing research program, the present paper further examines the flow on the LD9 unit using, instead, the commercial CFD program, FLUENT, and the more robust Volume-of-Fluid (VOF) method for modelling the free surface transport. This paper extends the preliminary qualitative fluid flow study of Matthews *et al.* (1996) in which only laminar solutions were presented. Quantitative fluid flow predictions have now been achieved using the RNG k-ε turbulence model and particulate flow analyses have also been conducted at dilute concentration.

2. MATHEMATICAL FORMULATION

2.1 Fluid flow

Studies by Holland-Batt (1989) and Holtham (1990) have demonstrated that spiral concentrator flows possess a free-surface, have shallow depths of typically less than 1 cm and display laminar to increasingly turbulent behaviour radially outwards across the trough with velocities reaching 3 m/s. A secondary circulation current in a plane perpendicular to the mainstream flow direction, induced by the

spiral curvature and resultant centrifugal force, travels outwards near the free-surface and back inwards towards the central column near the trough base. To model this flow, the fluid phase is considered Newtonian, to possess constant physical properties and to be governed by the Reynolds-averaged turbulent Navier-Stokes equations. The steady-state equations for the conservation of mass and momentum in generalised curvilinear form, are respectively given by:

$$\frac{\partial \rho_f u_f^i}{\partial x_i} = 0 \qquad (1)$$

$$\frac{\partial}{\partial x_j}\left(\rho_f u_f^i u_f^j\right) = -\frac{\partial P}{\partial x_i} + \rho_f g_i + \frac{\partial}{\partial x_j}\left[\mu_{eff}\left(\frac{\partial u_f^i}{\partial x_j} + \frac{\partial u_f^j}{\partial x_i}\right)\right] \qquad (2)$$

where ρ_f is the fluid density, μ_{eff} the effective (molecular μ plus turbulent μ_t) viscosity, P the static pressure, and $u^{i,j}$ and g_i the mean velocity and gravitational acceleration, respectively. To consider the effects of turbulence, the eddy viscosity concept and dynamic renormalisation group theory (RNG) based k-ε turbulence model (Yakhot and Orzag, 1986) have been employed. This model contains very few empirically adjustable parameters and is therefore applicable to a wide range of flow situations. The local level of turbulent kinetic energy (k) and energy dissipation rate (ε) are solved using the following transport equations:

$$\rho_f \frac{\partial\left(u_f^j k\right)}{\partial x_j} = \frac{\partial}{\partial x_j}\left(\alpha\mu_t \frac{\partial k}{\partial x_j}\right) + P_k - \rho_f \varepsilon \qquad (3)$$

$$\rho_f \frac{\partial\left(u_f^j \varepsilon\right)}{\partial x_j} = \frac{\partial}{\partial x_j}\left(\alpha\mu_t \frac{\partial \varepsilon}{\partial x_j}\right) + \frac{\varepsilon}{k}\left(C_1\mu_t P_k - C_2\rho_f \varepsilon\right) - R \qquad (4)$$

where P_k is the turbulence production and R an additional rate of strain term. According to the RNG theory, the constants in the turbulent transport equations are given as $C_1 = 1.42$ and $C_2 = 1.68$. The variable α is solved throughout the domain and takes into account both the high and low Reynolds number regions and effects due to streamline curvature.

The free-surface transport has been modelled using the Volume-of-Fluid (VOF) method (Hirt and Nichols, 1981). In this technique, the interface between water and air is tracked on a fixed mesh so that the interface does not generally coincide with a grid line. A function F is defined whose value is unity at any point occupied by fluid and zero otherwise. The average value of F in a cell represents the fractional volume of that cell occupied by the fluid with values between zero and one containing the free-surface. Evolution of the F field is governed by the following transport equation:

$$\frac{\partial F}{\partial t} + u_f^i \frac{\partial F}{\partial x_i} = 0 \qquad (5)$$

After the distribution of F has been determined, the interface in each cell is reconstructed from the cell value and local gradient of F. The velocities and pressure in cells which contain the interface are then assigned to ensure satisfaction of the complete free surface stress conditions (Nichols and Hirt, 1971). Because the flow field calculations are not coupled with determination of the free-surface location, the VOF method provides a more stable alternative to the adaptive-grid formulation used by Jancar *et al.* (1995). The model of Jancar has had difficulty in attaining spiral flow solutions with high free-surface curvature and hence appears somewhat limited for predictive design purposes (Matthews *et al.*, 1996) .

To solve (1) to (5), appropriate boundary conditions must be employed in the flow domain. At the spiral inlet all fluid velocity components have been specified and the distribution of F defined to give a desired flow rate. At the exit, mainstream gradients of the velocity components have been set to zero and no-slip conditions imposed at solid surfaces. The non-equilibrium wall function has been used to link the flow with the near wall profiles of velocity and turbulence parameters.

2.2 Particulate flow

In this paper, the Lagrangian method has been used to simulate the particulate flow at dilute

concentration on the LD9 spiral. The trajectory of an individual dispersed particle is calculated by integration of the force balance on the particle to equate its inertia and, in curvilinear non-orthogonal form, this balance may be expressed by (Maxey and Riley, 1983):

$$\frac{du_p^i}{dt} = \left(\frac{\rho_f}{\rho_p}\right) u_p^i \frac{\partial u_f^i}{\partial x_i} + \frac{1}{2}\frac{\rho_f}{\rho_p}\frac{d}{dt}\left(u_f^i - u_p^i\right) + \frac{3\mu_f C_D Re_p}{4\rho_p D_p^2}\left(u_f^i - u_p^i\right) + \left(\frac{\rho_p - \rho_f}{\rho_p}\right) g_i \quad (6)$$

where Re_p is the particle Reynolds number, D_p the particle diameter and C_D a drag coefficient. The forces on the right-hand-side of (6) represent respectively, the pressure gradient in the fluid, "virtual mass" required to accelerate the fluid surrounding the particle, Stokes steady-state viscous drag, and buoyancy due to gravity. To predict the particulate dispersion due to turbulence and crossing trajectory effect due to gravity, a stochastic Continuous Random Walk model (Thomson, 1987) has been used. Preliminary simulations of the particle-wall interaction have used a simple collision model with a restitution coefficient of 1.0 assumed.

3. NUMERICAL PROCEDURE

The LD9 computational domain uses a single block, structured, curvilinear 3D grid. For computing purposes, the spiral has been divided into 35° sections (Figure 1) with the computed outlet solution specified as the inlet conditions for the next downstream sector. The domain is bounded by four walls and the flow is essentially a duct flow that includes an interface between water and air. The model irrelevantly calculates the air flow solution but because grid cells are stretched in the depth-wise direction toward the spiral base, the computing time to do this is minimised.

Equations (1) - (5) have been solved using a finite volume method on a non-staggered grid. The primitive flow field and VOF distributions were solved implicitly in which the convective first derivatives in (2) and (5) were calculated using a second-order QUICK discretisation scheme; three point symmetrical formulae were used to discretise the second derivatives. The velocity fields were determined from (2) using the iterative Line-Gauss-Seidel scheme and a velocity potential correction introduced to satisfy continuity (1) and to upgrade the pressure field using the SIMPLE algorithm.

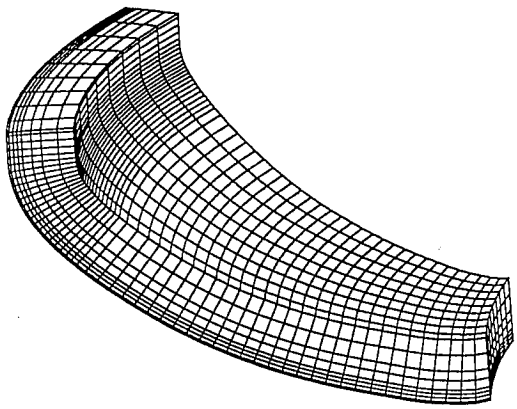

Figure 1 The LD9 computational domain with reduced cells for clarity

After the volume fraction F had been calculated and the free surface position located, boundary conditions at the interface were used to determine the pressure and velocities within the surface cells. The primitive flow variables were then updated and the process repeated until neither the flow field nor the free surface profile changed. For this purpose, all residuals were reduced to below 3×10^{-4} before transfer of the outlet results to the inlet plane of the next downstream sector. Typically, CPU times of four hours were required to reach the fully-developed state and a further two hours needed to transfer the results downstream on a Hewlett-Packard K210 Unix server.

Use of only the QUICK scheme in the solution process would have led to progressive smearing of the F function and loss of definition of the interface by dissipative and dispersive terms occurring in the truncation error. Accordingly, the Donor-Acceptor method (Hirt and Nichols, 1981) was used to compute F explicitly using a time-marching scheme after convergence in each sector. Typically, 50 time-steps of 0.001s were needed for the interface to be convected from the inlet to outlet plane. In the Donor-Acceptor method, sharper resolution is attained by limiting the amount of fluid that can be convected across a cell face to the minimum of two values: the filled volume of the phase in the donor cell; or the free volume available in the acceptor cell.

The trajectories of individual particles were calculated in the fully-developed fluid flow domains for six complete spiral turns. Step-wise integrations over discrete time-steps were conducted using the Runge-Kutta method. Integration of (6) yielded the velocity of the particle at each point along the trajectory and a further integration in time predicted the trajectory itself. The fluid velocity at the precise particulate position, estimated by a Taylor series expansion about the value stored at the cell-centre, was employed. Instantaneous values of the fluid velocity were also used and the trajectories of 100 particles with the same density and size calculated to account for the random effects of turbulence.

5. RESULTS

Analyses have been performed by examining the free-surface flow on the LD9 spiral unit at flow rates of 4, 6 and 8 m^3/hr. Substantial empirical data is available for validation of the model, comprising the work of Holtham (1990) and the collaborative experimental program (Golab *et al.*, 1997). In the present study, the 35° section of the spiral domain (Figure 1) consists of a mesh with 20 x 39-46 x 208 control volumes in the mainstream, depth-wise and radial directions, respectively. The number of cells in the depth-wise direction has been varied according to the flow rate and these cells have been clustered toward the spiral base so that in the region of maximum water depth, 22-37 of the 39-46 cells contain water.

The fully-developed fluid flow profile at 6m^3/hr is depicted in Figure 2. Induced by the centrifugal force, the water concentrates to the outer 20% of the spiral and smoothly increases its depth (0 to 7.8 mm) outwards across the trough. Predicted and measured depths against radial distance (4 and 8 m^3/hr) are plotted in Figure 3, in which the radial extent of water movement up along the outer wall is seen to be satisfactorily predicted. The most significant variation in depth between flow rates exists in the outer zones whilst in the inner regions, depths remain relatively uniform. Maximum predicted depths of 5.5, 7.8 and 10.3 mm are less than those measured (Figure 3) although in light of the unsteady flow nature (Holtham, 1990) and, perhaps more importantly, that the presence of finely dispersed entrained air within the turbulent outer regions may have resulted in significant error of the conductivity depth measurements (Holland-Batt and Holtham, 1991), the comparisons are probably within acceptable limits of the numerical and experimental uncertainties.

In the experimental analysis of Holtham (1990), flow regimes across the trough were calculated using the relationship for Reynolds number, *Re*, in open channel flow, given by: $Re = \rho h V_M / \mu$ in which h is the local mean flow depth (Figure 3) and V_M the mean velocity. Values of V_M for 8 radial streams were determined by dividing the spiral into sections using vertical splitter plates, measuring the flow rates in each stream and estimating their cross-sectional area. Assuming that the transition from laminar to turbulent flow occurs in the range $400 < Re < 2000$, the transition supported by the injection of dye traces, was found to occur at 0.08-0.16 m radius with estimated error bounds of ±30%. Similarly, the computational equivalent of *Re* at 4 m^3/hr predicts the transition to occur at 0.04-0.14 m from the central column (Figure 4).

Measurements of instantaneous mainstream velocities on the LD9 unit have recently been enabled using Particle Image Velocimetry (Golab *et al.*, 1997). The measurements are estimated to have reasonably small error (± 20%), allowing the value of any given theoretical model to be rigorously assessed. Similar to the empirical analysis, our model predicts the mainstream velocity to smoothly increase in magnitude outwards across the trough; the velocity distribution at 6 m^3/hr is depicted in Figure 2. In general, the maximum velocity at any given radius occurs at the free-surface and increases from ~0.3 m/s in the innermost trough region to its highest value at ~95% of the outer radius. Encouragingly, the maximum predicted values of 2.0, 2.4 and 2.6 m/s at respectively, 4, 6 and 8 m^3/hr compare well with the equivalent measured velocities of 2.0, 2.3 and 2.2 m/s.

Perhaps the greatest test for quantitative purposes is comparison of the instantaneous velocities for a range of radii and depths within the flow. Simulations of the mainstream velocity at 4 m^3/hr for flow depths of 1, 3 and 5

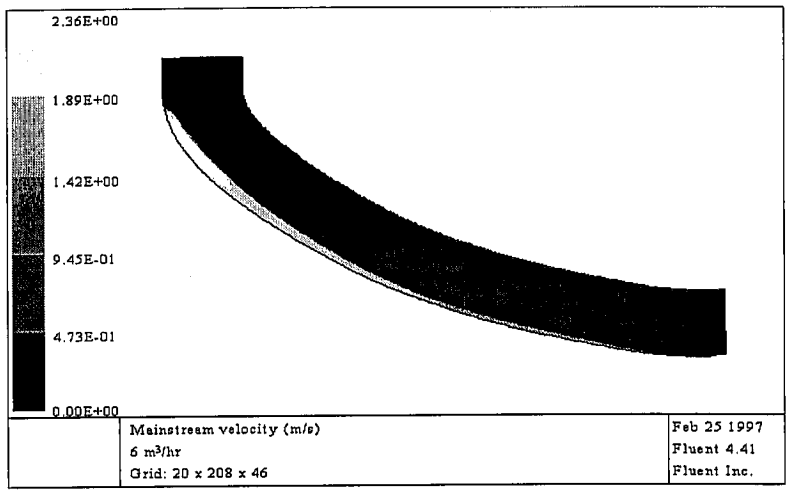

Figure 2 Predicted fluid profile and mainstream velocity distribution at $6m^3/hr$

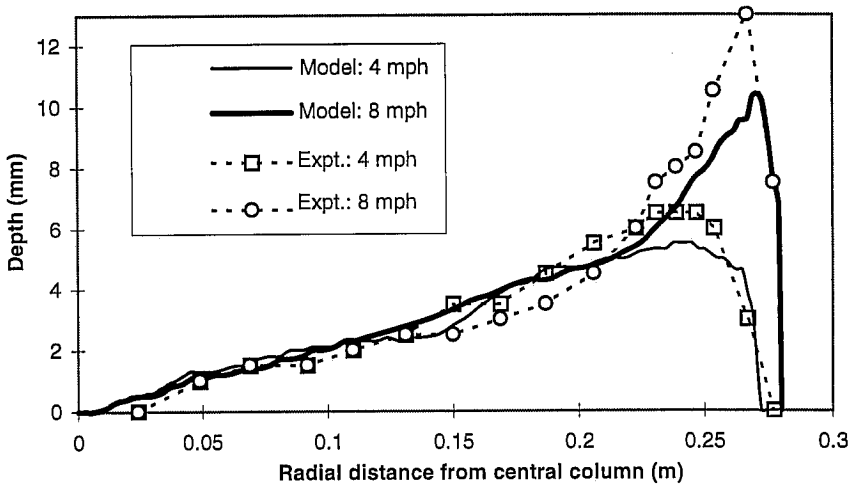

Figure 3 Fluid depth profiles: experiment versus model at flow rates of 4 and 8 m^3/hr

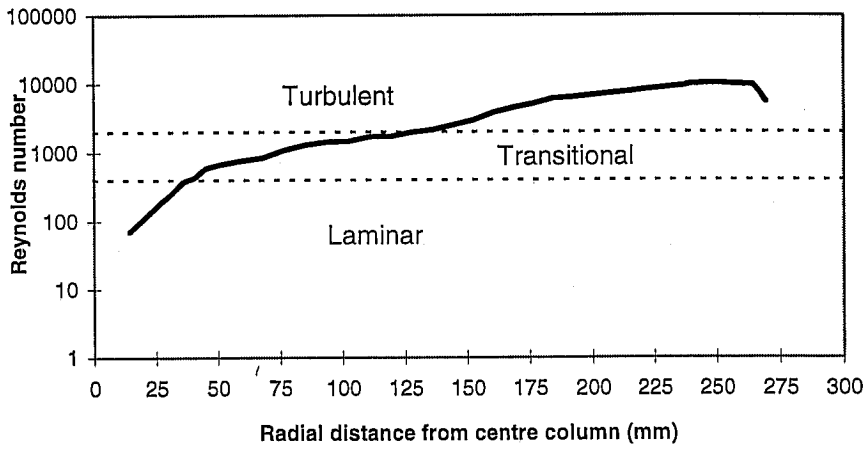

Figure 4 Predicted Reynolds number versus radial distance at $4m^3/hr$

mm are plotted in Figure 5. Measurements are also given with velocities at depths of 3-5 mm grouped together and error bars depicting 1 standard deviation about the mean values. Overall, very satisfactory agreement is found. Significant variation of the empirical data observed in Figure 5 probably reflects a number of causes, including the genuine physical transient nature of the flow, the inclusion of anomalous data points in the analysis which have yet to be discounted, and the error associated in resolving the depths to within only 0.5 mm (Golab *et al.*, 1997).

The model is able to capture the secondary fluid flow, the structure of which in the outer region of the spiral is depicted in Figure 6 at 8 m^3/hr. In general, the flow is seen to move outwards at the free-surface and back inwards toward the central column near the trough base with the flow reversal occurring at fractional depths of 0.4-0.5. Unlike the predicted mainstream velocity profiles, the secondary flow is distinctly unsteady in magnitude with variations of ± 20%. Its magnitude is approximately an order of magnitude less than the mainstream component with mean predicted maximums at 4, 6 and 8 m^3/hr of 0.13, 0.2 and 0.22 m/s, respectively. Preliminary empirical data are consistent with these results although the transient variations are much greater and of at least the same order as the mean values (Golab *et al.*, 1997). At the highest flow rate a reverse circulation current, yet to be measured by experiment, is predicted in the outer region. Similar reverse flow structures in curved channels have been measured and predicted in other studies (e.g. De Vriend, 1981; Jayanti *et al.*, 1990).

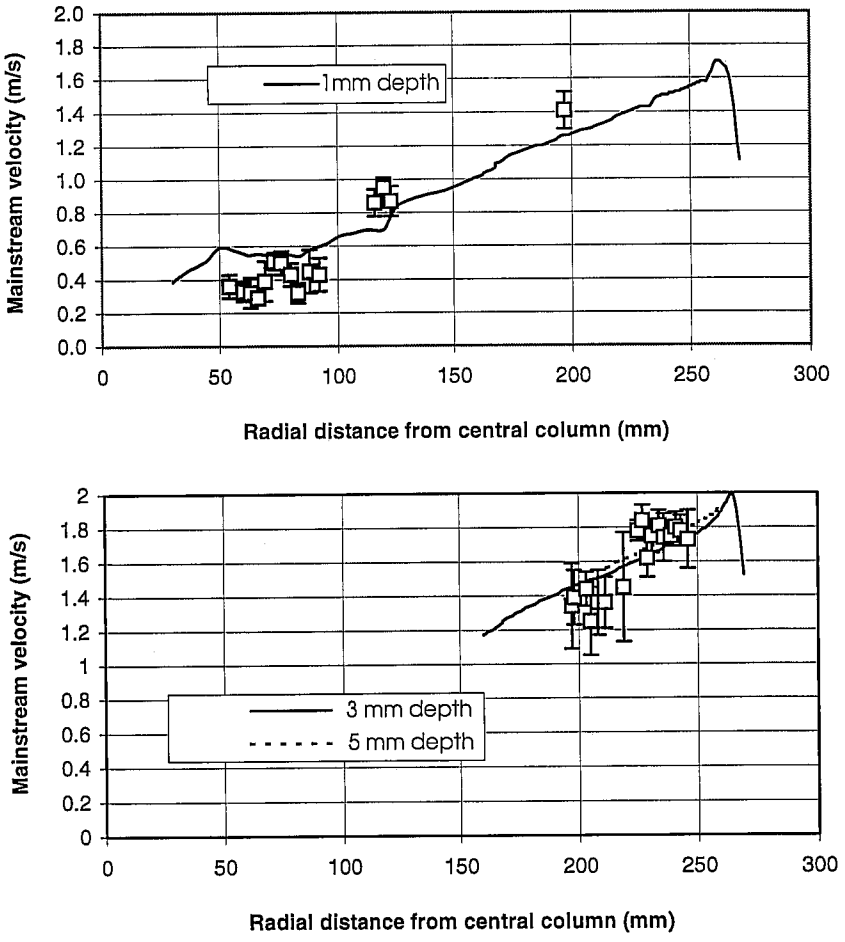

Figure 5 Predicted and measured mainstream velocities: 1mm depth (top); 3-5 mm depth (lower). Curves are numerical predictions. Measured values represent means of 4-12 points.

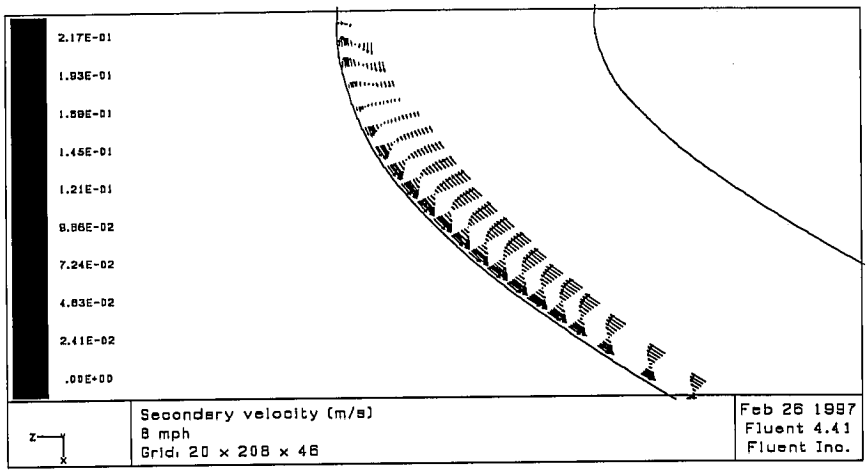

Figure 6 Secondary flow in the outer trough at a flow rate of 8 m^3/hr. The number of vectors have been reduced by respectively, factors of two and four in the depth-wise and cross-stream directions.

To examine the hydrodynamic influences on relative particulate separation, 100 particles have been input into the flow domains at 4 and 8 m^3/hr. Distributions across the trough were determined after the particles had travelled six complete turns down the spiral. Preliminary analyses have been performed for both coal particles (ρ_p = 1450 kg/m^3) and quartz (ρ_p = 2650 kg/m^3) which represent the extremes of density processed on the LD9 unit. The full range of particle sizes (100 - 1500 μm) were also examined. Unfortunately, data from the collaborative experimental program is not yet available to compare with the numerical simulations.

The predicted distributions clearly demonstrate the classic pattern observed on spiral separators with finer and less dense particles migrating to the outer trough zones. Similarly to the numerical study of Holland-Batt (1989), outward migration diminished rapidly above 500 μm for both particulate densities and flow rates. Above this limit, the particles were found to accumulate within the innermost region. Under all conditions the finest (100 μm) particles migrated to the outer zones whilst variations of flow rate and density were found to influence particles in the somewhat narrow size range of 100 < D_p < 500 μm on the LD9 unit. Distributions for the 200 μm coal and quartz particles at both flow rates are presented in Figure 7.

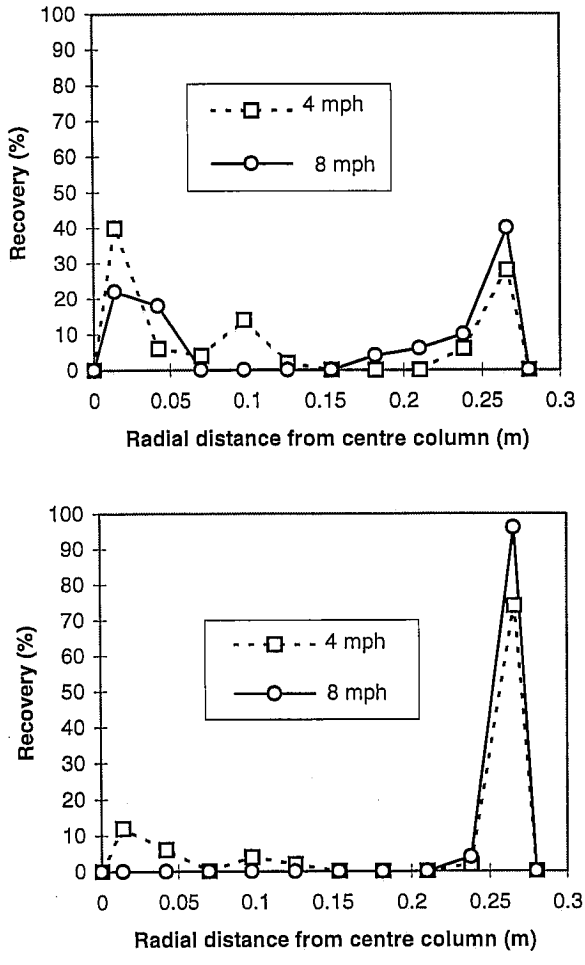

Figure 7 Predicted radial distributions for 200 μm particles of quartz (top) and coal (bottom) at flow rates of 4 and 8 m^3/hr

Simulations of the fluid secondary velocity distribution have shown that the circulation at 8 m^3/hr is significantly stronger than at 4 m^3/hr with predicted maximum values of respectively, 0.13 and 0.22 m/s. Because the secondary velocity primarily drives the process of particulate separation (Holtham, 1990), it is to be expected that greater outward migration would occur at 8 m^3/hr. This is seen to be the case for particles of 200 μm diameter (Figure 7) although the distributions appear to be more sensitive to variations in density than the flow rate.

6. CONCLUSIONS

A commercially available CFD code, FLUENT, has been used to model the fluid and dilute particulate flow on the LD9 spiral used for fine coal processing. For a range of flow rates, the free surface flow has been simulated using a robust fixed-grid Volume of Fluid method and RNG k-ε turbulence model. Sound quantitative agreement with experimental data has been obtained with respect to flow depths and, most encouragingly, instantaneous mainstream velocities at arbitrary radii and depths within the flow. The secondary current has been able to be captured, the magnitudes of which are of the same order as preliminary empirical data. Particulate analyses using the Lagrangian method have displayed the correct qualitative flow behaviour but have yet to be compared quantitatively with the collaborative experimental program. Future developments of the model will focus upon the particulate phase at progressively higher and hence more realistic feed concentrations.

REFERENCES

De Vriend, H.J., 1981, 'Velocity redistribution in curved rectangular channels', *J. Fluid. Mech.*, 107, pp. 423-439.

Golab, K.J., Holtham, P.N., Wu, J., 1997, 'Validation of a computer model of fluid flow on the spiral separator', *Innovation in physical separation technologies, Richard Mozely Memorial Symp., Inst. Min. Metall.*, London.

Hirt, C.W., Nichols, B.D., 1981, 'Volume of Fluid (VOF) method for the dynamics of free boundaries', *J. Comp. Phy.*, 39, pp. 201-225.

Holland-Batt, A.B., 1989, 'Spiral separation: theory and simulation', *Trans. Instn. Min. Metall. (Sect. C)*, 98, pp. C46-60.

Holland-Batt, A.B., Holtham, P.N., 1991, 'Particle and fluid motion on spiral separators', *Minerals Engineering*, 4(3/4), pp. 457-482.

Holtham, P.N., 1990, 'The fluid flow pattern and particle motion on spiral separators', Ph.D. Thesis, University of New South Wales.

Jancar, T., Fletcher, C.A.J., Holtham, P.N., Reizes, J.A., 1995, 'Computational and experimental investigation of spiral separator hydrodynamics', *Proc. XIX Int. Mineral Proc. Congress*, San Francisco.

Jayanti, S., Hewitt, G.F., Kightley, J.R., 1990, 'Fluid flow in curved ducts', *Int. J. Num. Meth. Fluids*, 10, pp. 569-589.

Matthews, B.W., Fletcher, C.A.J., Partridge, A.C., Jancar, T., 1996, 'Computational simulation of spiral concentrator flows in the mineral processing industry', *Proc. CHEMECA '96, Aust. Inst. Chem. Engng.*, Sydney,

Maxey, M.R., Riley, J.R., 1983, 'Equation of motion for a small rigid sphere in a non-uniform flow', *Phys. Fluids*, 26(4), pp. 883-889.

Nichols, B.D., Hirt, C.W., 1971, 'Improved free surface boundary conditions for numerical incompressible-flow calculations', *J. Comp. Phy.*, 8, pp. 434-448.

Thomson, D.J., 1987, 'Criteria for the selection of stochastic models of particle trajectories in turbulent flows', *J. Fluid. Mech.*, 180, pp. 529-556.

Wang, J.W., Andrews, J.R.G., 1994, 'Numerical simulation of liquid flow on spiral concentrators', *Minerals Engineering*, 7, pp. 1363-1386.

Yakhot, V., Orszag, S.A., 1986, 'Renormalisation group analysis of turbulence', I. Basic theory, *J. Sci. Comput.*, 1(1), pp. 1-51.